The Enzymatic Oxidation of Graphene Oxide

Gregg P. Kotchey,[†] Brett L. Allen,[†] Harindra Vedala,[†] Naveena Yanamala,[‡,§] Alexander A. Kapralov,[‡] Yulia Y. Tyurina,[‡] Judith Klein-Seetharaman,[§] Valerian E. Kagan,[‡] and Alexander Star[†,*]

[†]Department of Chemistry, [‡]Department of Environmental and Occupational Health, and [§]Department of Structural Biology, University of Pittsburgh, Pittsburgh, Pennsylvania, 15260

ABSTRACT Two-dimensional graphitic carbon is a new material with many emerging applications, and studying its chemical properties is an important goal. Here, we reported a new phenomenon—the enzymatic oxidation of a single layer of graphitic carbon by horseradish peroxidase (HRP). In the presence of low concentrations of hydrogen peroxide (~40 μM), HRP catalyzed the oxidation of graphene oxide, which resulted in the formation of holes on its basal plane. During the same period of analysis, HRP failed to oxidize chemically reduced graphene oxide (RGO). The enzymatic oxidation was characterized by Raman, ultraviolet-visible, electron paramagnetic resonance, Fourier transform infrared spectroscopy, transmission electron microscopy, atomic force microscopy, sodium dodecyl sulfate-polyacrylamide gel electrophoresis, and gas chromatography−mass spectrometry. Computational docking studies indicated that HRP was preferentially bound to the basal plane rather than the edge for both graphene oxide and RGO. Owing to the more dynamic nature of HRP on graphene oxide, the heme active site of HRP was in closer proximity to graphene oxide compared to RGO, thereby facilitating the oxidation of the basal plane of graphene oxide. We also studied the electronic properties of the reduced intermediate product, holey reduced graphene oxide (hRGO), using field-effect transistor (FET) measurements. While RGO exhibited a V-shaped transfer characteristic similar to a single layer of graphene that was attributed to its zero band gap, hRGO demonstrated a p-type semiconducting behavior with a positive shift in the Dirac points. This p-type behavior rendered hRGO, which can be conceptualized as interconnected graphene nanoribbons, as a potentially attractive material for FET sensors.

KEYWORDS: graphene · oxidation · microscopy · peroxidase · field-effect transistor

Graphene has captured the attention of the scientific community due to its novel electronic properties[1,2] coupled with its mechanical strength,[2,3] both of which may make graphene integral in future generations of electronics, batteries, sensors, and composites.[1,2,4−6] One of the current methods of synthesizing graphene entails exfoliating graphite through oxidation to yield graphite oxide (GO), and this material is sonicated to produce graphene oxide.[7,8] Graphene oxide is subsequently reduced either chemically[7−10] or thermally[7,11,12] to produce reduced graphene oxide (RGO).

While the graphene precursor, GO, has been studied for about 170 years,[13] now there is emerging interest in graphene oxide and RGO.[14−18] For example, graphene oxide has been proposed for drug delivery and cellular imaging applications.[14] Further, graphene oxide paper formed from interlocking sheets of graphene oxide demonstrated superior strength and stiffness compared to many other papers.[15] Finally, graphene oxide has been suggested as a simple alternative to poly-(3,4-ethylenedioxythiophene)-poly(styrenesulfonate) (PEDOT:PSS), a hole transporting layer and electron blocking layer in organic photovoltaics (OPVs).[16] RGO, on the other hand, has been employed for both chemical and biological sensing applications.[17,18] Given the recent rise in applications for graphene oxide and RGO, it is important to study the chemical properties of these carbon nanomaterials and to develop methods for their remediation to minimize their environmental impact.

Graphene and graphene derivatives such as graphene oxide have been modified for applications through treatment with strong oxidizing and reducing agents,[19] oxidative etching at temperatures greater than 400 °C,[20] etching using lithography,[21] and sonochemical approaches.[22] Here, we report an entirely new phenomenon; mild enzymatic oxidation resulted in the formation of holey graphene oxide nanostructures as demonstrated by numerous analytical techniques. Computational studies that complemented these results suggested that the molecular mechanisms for oxidation were related to the orientation, dynamics, and binding strength of the enzyme to different graphene sheets. In addition to reporting on the reactivity of graphene oxide and RGO toward oxidation by peroxidases, we also demonstrated that the enzymatic treatment of this graphitic nanomaterial resulted in alterations of their electronic properties. In particular, we found that holey reduced graphene oxide (hRGO), the reduced form of holey graphene oxide, demonstrated

* Address correspondence to astar@pitt.edu.

Received for review December 3, 2010 and accepted January 27, 2011.

Published online February 23, 2011
10.1021/nn103265h

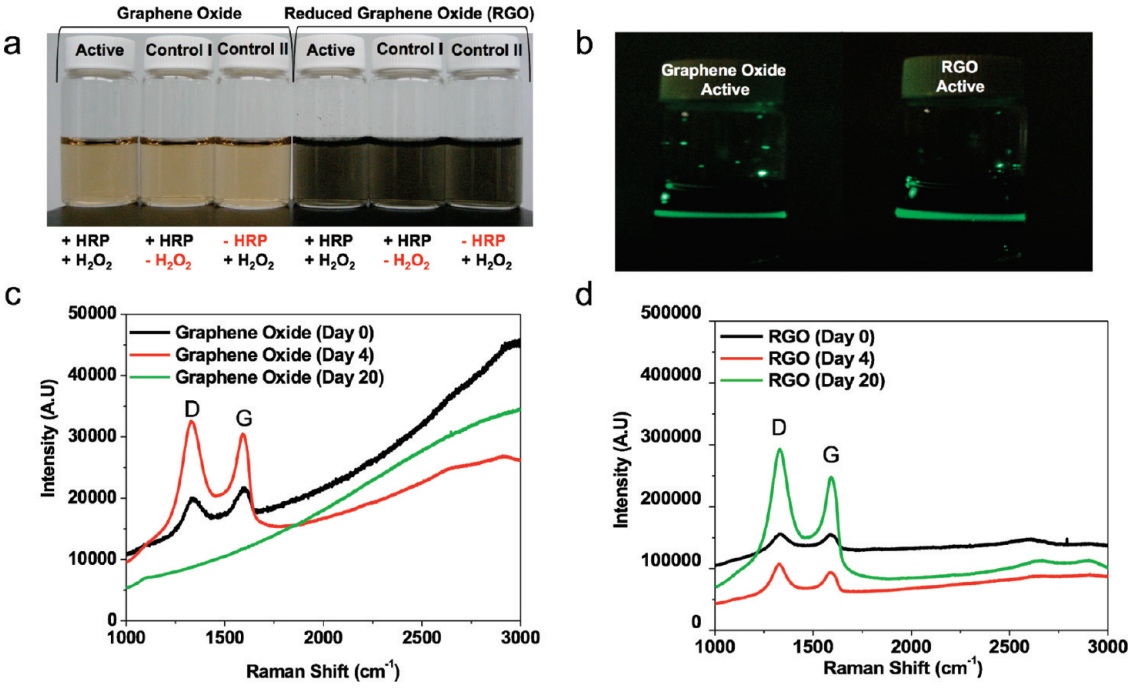

Figure 1. (a) Sample vials for the graphene oxide and RGO enzymatic oxidation experiment. (b) The Tyndall scattering effect confirmed that the dispersions that consist of either graphene oxide or RGO with HRP (at day 0 of the oxidation process) were colloids. Raman spectra depicting (c) graphene oxide and (d) RGO after days 0 (black), 4 (red), and 20 (green) of incubation with horseradish peroxidase (HRP)/H_2O_2. The D and G bands are marked on the spectrum.

p-type semiconducting behavior, which could make this material desirable for applications involving field-effect transistors (FETs).

RESULTS AND DISCUSSION

Enzymatic Reaction Conditions and Spectroscopic Analysis. Similar to our previous work where single-walled carbon nanotubes (SWNTs) were degraded *via* enzymatic catalysis,[23−25] both graphene oxide and RGO samples were incubated with horseradish peroxidase (HRP) at pH 7.0, room temperature, and low concentrations (~40 μM final concentration) of hydrogen peroxide (H_2O_2) that were added daily (Figure 1a). These dispersions, which consisted of either graphene oxide or RGO with HRP, were classified as colloids based on the Tyndall scattering effect (Figure 1b).[19] In addition, Raman spectroscopy was used to analyze graphene oxide and RGO on days 0, 4, and 20 of incubation with HRP/H_2O_2 (Figure 1c,d), and the ratio of the D band, which measured the presence of disorder in sp^2-hybridized carbon systems, to G band that evaluated stretching of C−C bonds in graphitic materials were compared.[26] For graphene oxide between days 0 and 4, the D:G ratio increased from 1.1:1.0 to 1.6:1.0, and by day 20, both the D and G bands disappeared. For RGO, the D:G ratio between day 0 and 4 decreased from 1.2:1.0 to 1.1:1.0, and increased to 1.3:1.0 by day 20. There were two plausible explanations for the increase in the D:G ratio from 1.1:1.0 to 1.6:1.0 between days 0 to 4 of graphene oxide incubation. First, because Raman spectroscopy was performed on different flakes, the variance in the D:G ratio may have been the result of different degrees of graphene oxide oxidation due to the modified Hummers' method. Second, there may have been an increase in the number of defect sites as a result of HRP catalyzed oxidation of the graphitic lattice. The D and G bands disappeared by day 20 as a result of the complete enzymatic oxidation of the graphitic lattice; therefore, Raman spectroscopy provided evidence that graphene oxide underwent oxidation. For RGO samples, Raman data in Figure 1d showed an increase in the D:G ratio after graphene oxide was reduced to RGO using hydrazine, similar to previous literature.[10] The fluctuations observed in the D:G ratio for RGO between days 0, 4, and 20 were attributed to variations in samples since different flakes were examined.

Microscopy. Transmission electron microscopy (TEM) was utilized to monitor the progression of HRP catalyzed oxidation of graphene oxide over a 20 day period with daily additions of 40 μM H_2O_2 (final concentration, Figure 2a). Initially at day 0, flat sheets with dimensions ranging from 0.5 to 1.5 μm were observed. After 5 days, graphene oxide sheets began to wrinkle; visible holes were formed in the graphitic lattice of the basal plane by day 8. The size of the holes increased with time; at day 8 the average hole size was 2.1 ± 0.6 nm *versus* 26.7 ± 12.8 nm at day 10 of the oxidation process (Figure 3). By day 12 as the hole size continued to expand, small flakes of graphene oxide were observed, and the majority of graphene oxide was completely oxidized by day 20 of the experiment (Figure 2a). In contrast, no oxidation was observed by TEM for the graphene oxide controls

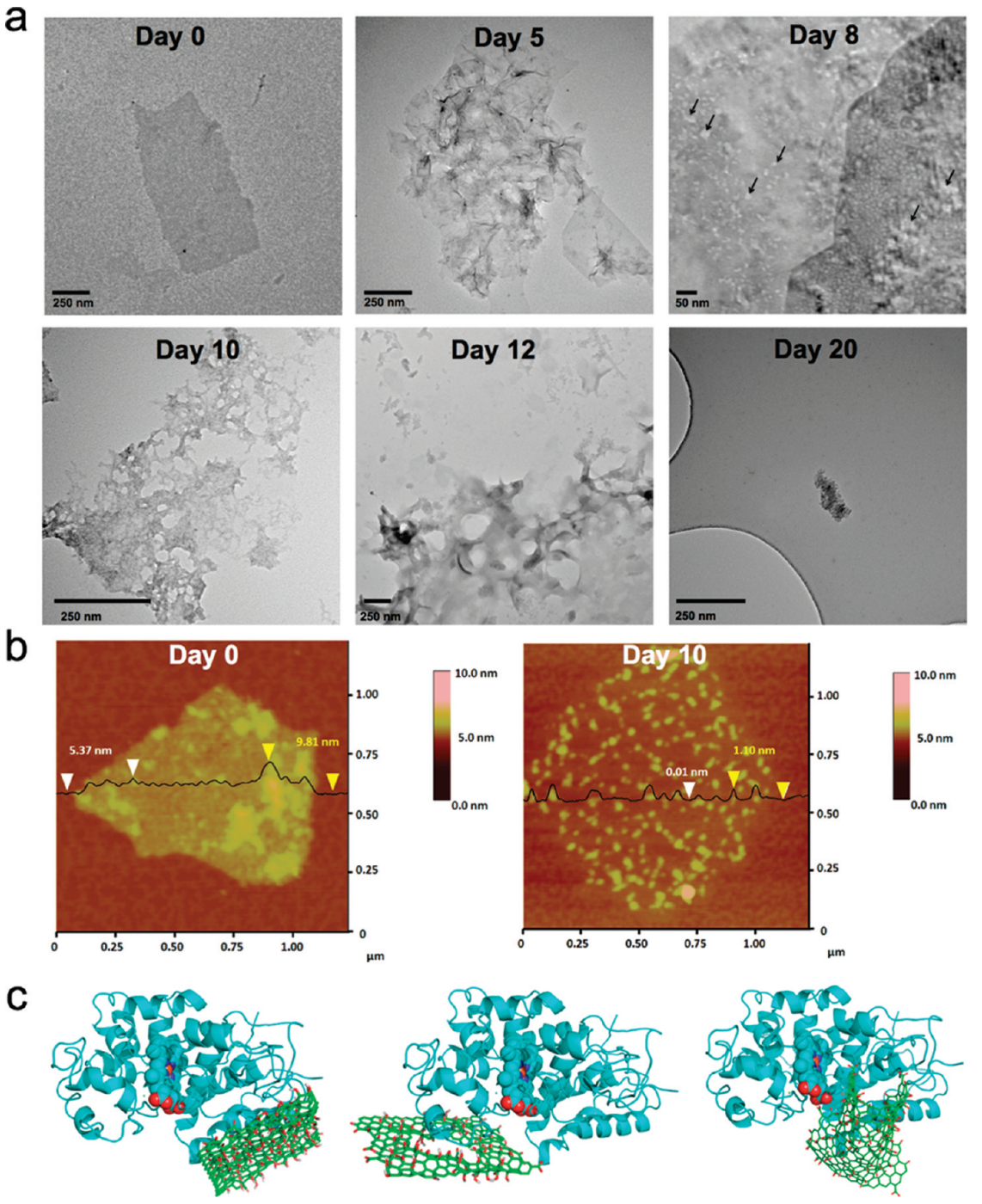

Figure 2. (a) TEM micrographs of graphene oxide after 0, 5, 8, 10, 12, and 20 days of incubation with HRP and 40 μM H_2O_2. Arrows indicate hole formation in the basal plane at day 8. (b) Atomic force microscopy (AFM) images with section analysis of graphene oxide with HRP at day 0 (left) and holey graphene oxide at day 10 (right). Graphene oxide with HRP has a sheet height of 5.37 and 9.81 nm. Holey graphene oxide has a sheet height of 1.10 nm, and the holes were authentic at a height of 0.01 nm. (c) Binding poses of HRP on (from left to right) graphene oxide, holey graphene oxide, and a small sheet of graphene oxide calculated using molecular docking studies (AutoDock Vina).

($-H_2O_2$, Supporting Information, Figure S1a and $-$HRP, Figure S1b). From the TEM micrographs obtained over the 20-day period of the study, it was concluded that graphene oxide underwent significant oxidation, which resulted in the formation of holes on its basal plane.

The TEM micrographs of graphene oxide at day 8 and 10 of the oxidation process were scrutinized to obtain information regarding the oxidation mechanism. In particular, two parameters were analyzed: the neck width (*D*) and the hole diameter (*d*) (Figure 3 insert). Interestingly, as the diameters of the holes increased on average 12 times (2.1 $\pm$ 0.6 to 26.7 $\pm$ 12.8 nm) from days 8 to 10, the neck width remained roughly unchanged (9.4 $\pm$ 7.8 *versus* 8.9 $\pm$ 6.9 nm for

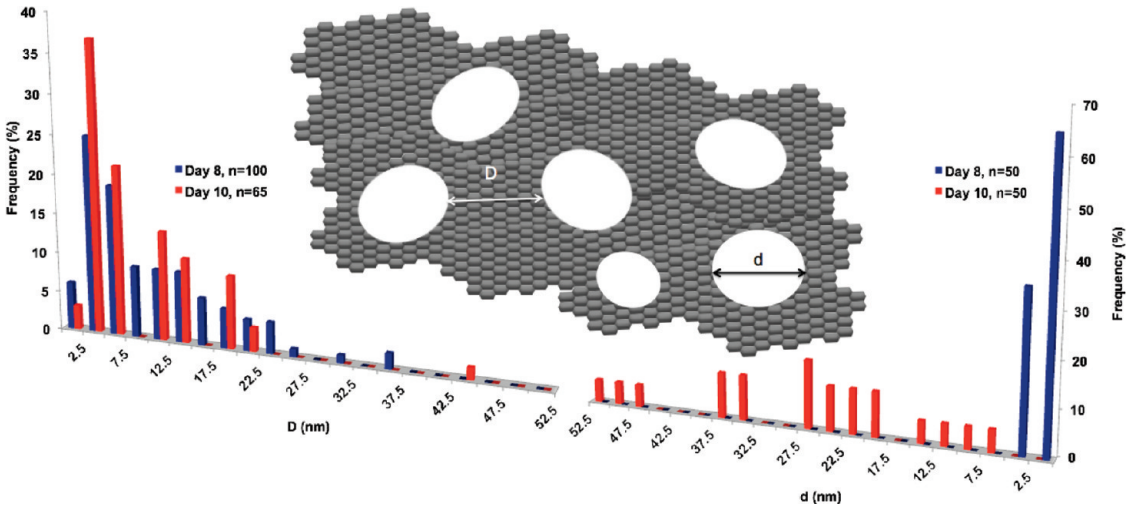

Figure 3. Histograms of neck width (*D*) and hole diameter (*d*) on days 8 and 10 of the oxidation process as measured from TEM micrographs. The cartoon insert illustrates the definitions of neck width and hole diameter.

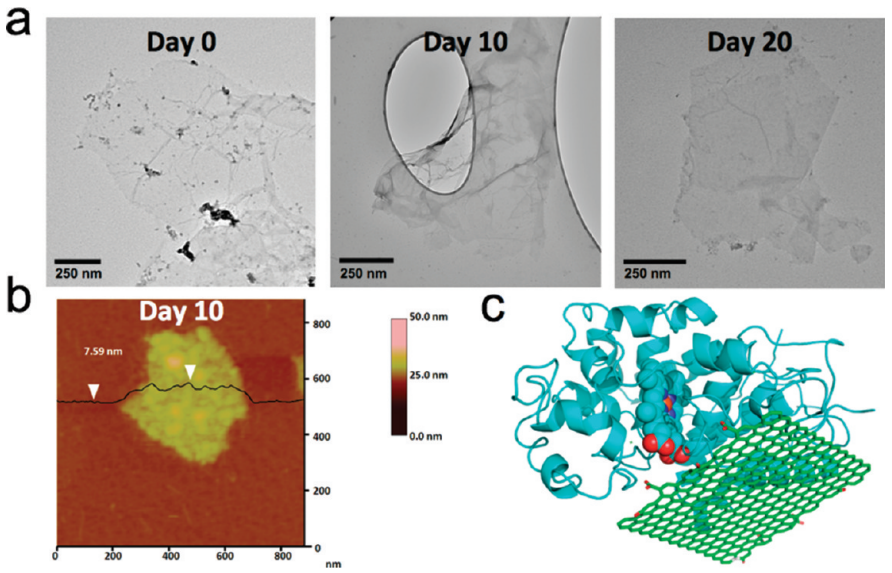

Figure 4. (a) TEM micrographs of RGO after 0, 10, and 20 days of incubation with HRP and 40 μM H_2O_2. (b) AFM images with section analysis of RGO with HRP at day 10. RGO with HRP has a sheet height of 7.59 nm. (c) Binding poses of HRP on RGO calculated using molecular docking studies (AutoDock Vina).

days 8 and 10, respectively). This implies that enzymatic oxidation cannot produce neck widths (*i.e.*, interconnected nanoribbons) smaller than a certain size. As the enzymatic oxidation reaction proceeded, the necks collapsed, which resulted in an increase in the diameters of the holes on average 12 times from days 8 to 10; the neck width, however, remained roughly unchanged for days 8 and 10.

As judged by TEM, RGO incubated under identical reaction conditions as graphene oxide failed to undergo oxidation over the same 20-day period (Figure 4a, Supporting Information, Figure S1c,d). A colorimetric assay performed with Amplex Red, a reagent commonly employed to measure trace H_2O_2 concentrations in biological systems,[27] had a peak for resorufin (the product of HRP catalyzed oxidation of Amplex Red) in the visible region around 570 nm for a sample containing RGO at both day 1 and day 20 of the oxidation process (Supporting Information, Figure S2). The assay revealed that at least a portion of HRP retained enzymatic activity in the presence of RGO; this observation was also confirmed by electron paramagnetic resonance spectroscopy (EPR, Supporting Information, Figure S3). Therefore, since there was no visible evidence of enzymatic oxidation for RGO over the 20-day period of analysis, it appeared that HRP interacted with RGO and graphene oxide differently (*vide infra*).

Graphene oxide, holey graphene oxide, and RGO were further examined by atomic force microscopy (AFM, Figures 2b and 4b, and Supporting Information, Figure S4). AFM section analysis indicated that graphene oxide had a height of 0.61 nm (Supporting Information, Figure S4a); therefore, the exfoliation of GO by sonication successfully produced a single layer

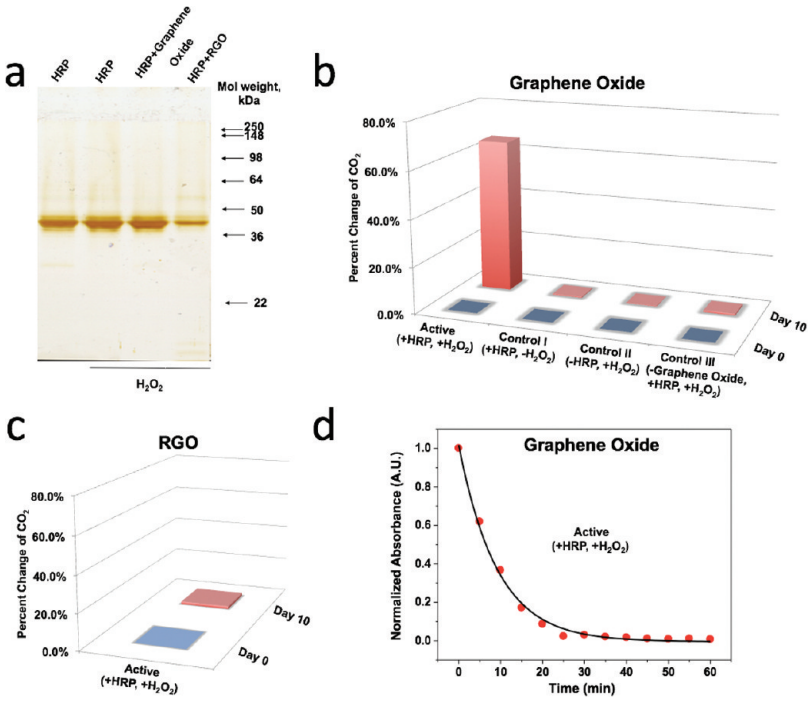

Figure 5. (a) SDS-PAGE with silver staining. The gel contained a control for HRP (around 44 kDa) without H_2O_2, HRP incubated for 3 hours in the presence of H_2O_2 (final concentration of 40 μM H_2O_2 added every 1 h), and HRP incubated with graphene oxide or RGO for 3 hours in the presence of H_2O_2 (final concentration of 40 μM H_2O_2 added every 1 h). A mass of 1.1 mg of HRP was utilized per test. (b,c) Relative increase in headspace CO_2 concentration as measured by GC−MS for day 0 and 10 for (b) graphene oxide-active, control I (−H_2O_2), control II (−HRP), control III (−graphene oxide), and (c) RGO-active. It was determined that the CO_2 concentrations in the headspace of the sample vials increased by 65% for graphene oxide-active, <1% for graphene oxide-control I, graphene oxide-control II, and graphene oxide-control III, and 2% for RGO-active. (d) Examination of the enzymatic kinetics for the graphene oxide-active sample employing an Amplex Red assay, where the absorbance of resorufin, which was directly proportional to H_2O_2 concentration, was measured at 5-min time intervals for 1 h. The assay indicated that nearly all of the H_2O_2 was consumed over the first 30 min of analysis as graphene oxide was oxidized.

of graphene oxide. Since graphene sheets have a height of 0.34 nm, it was not possible for two sheets to be present (*i.e.*, 0.61 nm < 0.68 nm). The presence of covalently attached oxygen functional groups (tertiary alcohols and epoxides) that decorate the basal plane of graphene oxide might be responsible for the added thickness of the graphene oxide flake. In addition, AFM confirmed that HRP binds to graphene oxide (Figure 2b). The height of the HRP was determined by AFM section analysis to be approximately 5 nm (Supporting Information, Figure S4b);[24] therefore, the height of 5.37 nm obtained by section analysis in Figure 2b (graphene oxide−Day 0) indicated that a single layer enzyme was bound to an individual sheet of graphene oxide. Applying the same reasoning, one could conclude that two layers of enzyme existed on graphene oxide to produce a region where the height was 9.81 nm. The height of the holey graphene oxide sheet was 1.10 nm (a graphene oxide bilayer) with a hole height of 0.01 nm (Figure 2b, graphene oxide−Day 10). Finally, AFM section analysis indicated that RGO had a height of 1.73 nm, which demonstrated that RGO consisted of an aggregation of flakes (Supporting Information, Figure S4c). Since the oxygen functional groups on the basal plane were reduced, van der Waals forces dominated between the flakes of RGO resulting in the formation of aggregates. Similar to graphene oxide, AFM confirmed that HRP was bound to RGO during the incubation process; unlike graphene oxide, however, no evidence of oxidation was observed by AFM at day 10 (Figure 4b, RGO−Day 10). With a total height of 7.59 nm, one layer of enzyme was bound to a RGO aggregate that contained between four and seven sheets.

HRP Interaction with Graphene Oxide/RGO. The ability of HRP to bind with sheets of graphene oxide/RGO was confirmed by sodium dodecyl sulfate-polyacrylamide gel electrophoresis (SDS-PAGE), followed by silver staining, shown in Figure 5a. Due to its size, both graphene oxide and the highly hydrophobic RGO failed to migrate well during gel electrophoresis; therefore, the majority of the material was retained in the stacking region of the gel. The protein band at 44 kDa corresponded to the literature value for HRP.[28] While initially all samples contained 1.1 mg of HRP, the quantity of protein that remained postincubation with RGO was approximately three times less than the quantity of HRP present in other samples, which indicated that HRP was bound more tightly to RGO than graphene oxide. Additionally, the results of gel electrophoresis indicated that minimal auto-oxidation took place during both the tested incubation period and for 40 μM levels of H_2O_2. In the absence of exogenous

oxidizable substrates, monomeric hemoproteins form dimers, trimers, and other oligomers during the activation of their peroxidase. This stems from the recombination of protein-derived (likely, tyrosyl) radicals generated as reaction intermediates[29−31] and results in the formation of covalent cross-links that are nondissociable in SDS. Thus if HRP oligomers were formed in the reaction, they should have been detectable in the SDS gel. The lack of HRP oligomers indicated that H_2O_2-dependent cross-linking of the enzyme did not take place, and the oxidizing potential of the enzyme was directed toward graphene oxide/RGO oxidation.

Molecular Modeling Studies. Employing AutoDock Vina software,[32] molecular docking studies were performed to identify the manner by which HRP was bound to RGO and graphene oxide. Docking of RGO to HRP indicated that there existed only one binding site on HRP where RGO can bind (Figure 4c, Supporting Information, Table S1). The closest distance to the heme active site from RGO was 11.5 Å. The results for graphene oxide, on the other hand, indicated two different binding sites for graphene oxide on HRP. The first binding site was similar to the RGO binding site with participation of the additional residues Ala86, Glu88, Ser89, Pro92, and Lue299. The heme active site was predicted to be 12.8 Å away from the graphene oxide surface (Supporting Information, Table S1). In comparison to the first binding site, the heme active site in the case of the second binding site was predicted to be 8.7 Å away from the surface of graphene oxide (Figure 2c, Supporting Information, Table S1). When a hole was introduced into the graphene oxide sheet, we predicted only one binding site that consisted of HRP residues similar to that of the second binding site described for graphene oxide (Figure 2c). The overall predicted binding energy was −26.7 kcal mol^{-1} for RGO; the two binding sites on graphene oxide had binding energies of −24.8 and −22.4 kcal mol^{-1}, respectively. These results indicated that HRP may bind more tightly to RGO than to graphene oxide. This was consistent with the gel electrophoresis data, which indicated that two-thirds of the incubated HRP was bound to RGO and retained in the well. The difference in binding of HRP to graphene oxide as compared to RGO may be responsible for the observed oxidation. These findings are also in line with our previous observation of HRP binding to oxidized *versus* nonoxidized SWNTs, where we also observed a preference of the enzyme's active site to be in closer proximity to the binding interface in oxidized material than in nonoxidized material. Finally, it was observed experimentally that holes formed preferentially on the basal plane, which indicated that the enzyme was more favorably bound to and oxidized the planar portion of graphene oxide instead of the edge. This observation was consistent with the docking results that only identified favorable binding poses on the plane. Thus, it appeared that the edge failed to provide sufficient surface area for stabilization of the graphene−HRP interaction through hydrophobic contacts.

In summary, the molecular modeling studies suggest that the presence of epoxy groups and hydroxyl groups in the basal plane and the flexibility of the oxidized graphene sheet may be responsible for the preferential enzymatic oxidation of graphene oxide and holey graphene oxide *versus* RGO by HRP.

Molecular Mechanisms of Oxidation. No visible evidence of oxidation as determined by TEM was observed for RGO over the 20-day period of analysis. Both the Amplex Red assay and the EPR data confirmed that the enzyme, HRP, remained active in the presence of RGO; therefore, another mechanism was responsible for the lack of visible oxidation. On the basis of our prior work with oxidized SWNT degradation[23−25] and the results obtained from the computational study, a potential mechanism for graphene oxide/RGO oxidation was elucidated. Since the binding energy was greater for RGO than graphene oxide, it was possible that the oxygen groups on graphene oxide allowed the enzyme to be more dynamic, which brought the heme site in close proximity of graphene oxide. Conversely, as a result of tighter binding between RGO and HRP, the dynamic motion of the enzyme was retarded. Therefore, the heme active site of HRP was not in close proximity of the graphene lattice, which was necessary for oxidation to occur. Initially, HRP was inactive, where the heme peroxidase was in the ferric oxidation state. In the presence of hydrogen peroxide (H_2O_2), the heme active site underwent a protein-assisted conversion to a ferryl oxo iron (Fe^{4+}=O) porphyrin π cation radical known as Compound I.[33] Compound I was reduced back to the ferric state in two sequential, one-electron transfer steps. In the first step, the transient intermediate, Compound II, was produced; during this process, the porphyrin π cation radical was reduced while graphene oxide was oxidized. Graphene oxide underwent further oxidation when the ferryl oxo iron (Fe^{4+}=O) was subsequently reduced to the ferric state. During this process, the σ carbon−carbon bond of the tertiary hydroxyl and epoxide groups that were formed during the initial oxidization of graphite by $KMnO_4$ and H_2SO_4 were cleaved. This was consistent with the literature, where it was demonstrated that peroxidases have the ability to catalyze both epoxidation and cleavage of carbon−carbon bonds in the presence of H_2O_2.[34,35]

Oxidation Product Analysis. While identification of the intermediate products of graphene oxide oxidation is ongoing, product analysis in the sample headspace utilizing gas chromatography−mass spectrometry (GC−MS) indicated that CO_2 was the final product of complete enzymatic catalyzed oxidation. Sample headspace of sealed vials in which HRP was incubated with either graphene oxide (Figure 5b) or RGO (Figure 5c) was extracted, and the concentration of CO_2 was determined.

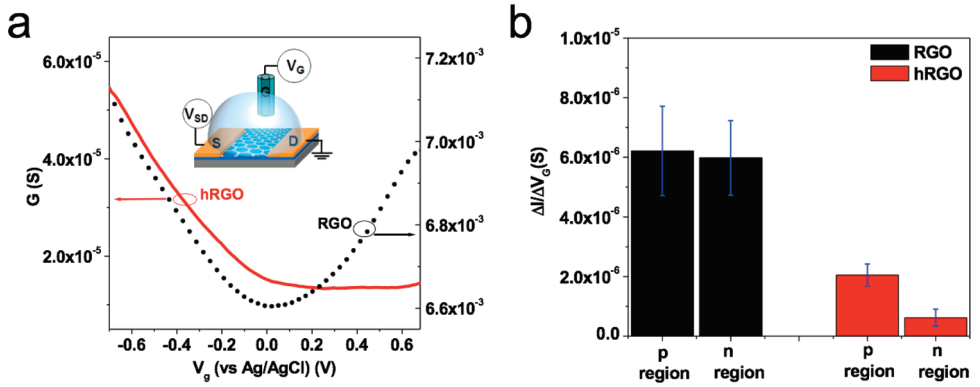

Figure 6. (a) Conductivity *versus* potential (liquid gate) plot for reduced graphene oxide (RGO, black circles) and holey reduced graphene oxide (hRGO, solid red line). The measurements were recorded in 10 mM KCl/10 mM PBS (pH 7) at a constant drain−source voltage of 10 mV. The inset represents a schematic of the experimental setup. (b) Comparison of transconductance ($\Delta I/\Delta V_g$) values of n and p region of 12 different RGO and hRGO FET devices (6 devices each).

By day 10, the concentration of CO_2 increased by 65% for graphene oxide (Figure 5b) and 2% for RGO (Figure 5c) over ambient; whereas the controls for graphene oxide (−HRP, $-H_2O_2$, and −graphene oxide) indicated only a <1% increase in relative CO_2 levels at day 10 (Figure 5b). With over 30 times the amount of CO_2 produced for graphene oxide oxidation compared to the RGO and the controls, the Raman and TEM results, which indicated that graphene oxide underwent HRP catalyzed oxidation, appeared to be substantiated.

Enzymatic Kinetics. Amplex Red was utilized to monitor the concentration of the substrate, H_2O_2, as a function of time to yield enzyme kinetics. HRP incubated with graphene oxide and H_2O_2 demonstrated that 97% of the substrate was consumed within 30 min (Figure 5d). It should be emphasized here that in all of the above experiments H_2O_2 was added on a daily basis to facilitate thorough characterization of the oxidation products. Taking into account the enzymatic kinetic data, we conducted additional experiments, where H_2O_2 was added every 30 min. For the resulting data, holes were observed in the basal plane of graphene oxide after 4.5 h (Supporting Information, Figure S1e). These results proved difficult to reproduce, however, due to the quick rate of enzymatic oxidation once holes were formed, rendering most of the graphene oxide "over-oxidized" (Supporting Information, Figure S1f). Attempts to shorten the total oxidation time by 15 min (*i.e.*, for a total oxidation time of 4.25 h) yielded pristine graphene oxide sheets; therefore, there existed a narrow window, where hole formation occurred. Consequently, with respect to reproducibly generating holey graphene oxide, the multiday approach appeared advantageous, and holey graphene oxide has been produced several times utilizing this technique.

Electronic Properties of Holey Reduced Graphene Oxide (hRGO). Creating holes in graphene is important for fine-tuning its electronic properties. As a result of its zero bandgap, graphene is a semimetal.[36,37] This property limits graphene's utility in some electronic applications such as room temperature FETs, which require semiconducting materials. To overcome this limitation, theoretical work has predicted that quantum confinement and edge effects would produce semiconducting properties at room temperature in graphene sheets that have widths less than 10 nm; an active area of graphene research involves the fabrication of these quasi-one-dimensional structures referred to as graphene nanoribbons (GNRs).[38−40] Block copolymer lithography,[41,42] laser induced photochemical reactions,[43] Joule heating,[44] oxidative etching at temperatures greater than 400 °C,[20] and two-dimensional polymer synthesis[45] have been employed to create nanometer sized holes on individual sheets of graphene. As a sheet of perforated graphene can be conceptualized as interconnected nanoribbons, the creation of holes in the basal plane of graphene opens its bandgap to yield a semiconducting nanomaterial.

To test if the sideproduct of enzymatic oxidation has unique electronic properties, holey graphene oxide that was formed after 8 days of oxidation was reduced with hydrazine to yield hRGO flakes (Supporting Information, Figure S1g), and this material demonstrated electrical conductivity. Both liquid-gated and back-gated FET measurements were implemented on RGO and hRGO (Figure 6a and Supporting Information, Figure S5a,b). For both of the measurement techniques, similar electronic transport characteristics were observed with the liquid gate measurement demonstrating more effective tuning of charge carriers.[46] RGO exhibited a V-shaped transfer characteristic (Figure 6a) similar to a single layer of graphene, which can be attributed to the zero band gap of graphene.[47−49] In comparison, hRGO exhibited a decrease in conductance with a p-type behavior and a positive shift in the Dirac points (Figure 6a). The comparison of transconductance ($\Delta I/\Delta V_g$) values for the n and p regions (Figure 6b) obtained from 12 different RGO and hRGO FET devices (6 devices each) confirmed the repeatability of the enhanced p-type semiconducting behavior of hRGO compared to RGO.

The observed p-type behavior for hRGO samples can be attributed to the presence of holes in the basal plane of the graphene nanomaterial, which resulted in the opening of the band gap as a consequence of lateral quantum confinement[38−40] and the presence of additional oxygen-containing functional moieties (*i.e.*, carboxylic acids, lactols, quinines, hydroquinones, *etc.*) around the holes that were introduced during the enzymatic oxidation process. These data were in accordance with recent reports on nanoperforated graphene.[41,42]

CONCLUSION

In this work, we demonstrated that HRP catalyzed the oxidation of graphene oxide that resulted in the formation of holes in the basal plane of this nanomaterial; over the same period of time, HRP failed to catalyze the oxidation of RGO. These observations were consistent with the computational findings, which indicated that the heme active site of HRP was in closer proximity, and the enzyme itself was more dynamic when bound to GO compared to RGO. This made graphene oxide more susceptible to carbon−carbon bond cleavage. With proposals for graphene oxide to be implemented in applications with an environmental impact,[50] the described enzymatic oxidation may be an attractive method for the bioremediation of graphene oxide. In addition to the environmental perspective, we discovered that enzymatic oxidation of graphene oxide produced holey graphene nanostructures, which upon reduction, demonstrated p-type semiconducting behavior. This material may have potential applications in electronic and sensor devices.

METHODS

Materials. Graphite flakes, lyophilized HRP type VI, PBS, hydrazine hydrate (50 wt %), and 30% H_2O_2 were purchased from Sigma Aldrich. Amplex Red was purchased from Molecular Probes, Invitrogen, and the SilverSNAP stain kit was acquired from Thermo Scientific.

Preparation of Graphene Oxide and RGO. Graphite oxide was prepared utilizing a modified Hummers' method on graphite flakes that underwent a preoxidation step.[51] Graphene oxide (∼0.125 wt %) was formed from graphite oxide that was diluted 1:4 with double distilled water and exfoliated for 30 min by ultrasonication followed by 30 min of centrifugation at 3400 rpm to remove unexfoliated graphite oxide. AFM, Fourier transform infrared spectroscopy (FT-IR), ultraviolet−visible spectroscopy (UV−vis), and TEM were employed to characterize the exfoliated graphene oxide. Graphene oxide had a sheet height of 0.61 nm, which was determined by section analysis and confirmed that a single layer of graphene oxide was present (Supporting Information, Figure S4a). Additionally, as evident by the FT-IR spectrum in Supporting Information, Figure S6a, major peaks appeared around 3400, 1700, and 1000 cm^{-1}, which were attributed to O−H, C═O, and C−O stretching vibrations, respectively. Moreover, Figure 2a depicted a single sheet of graphene oxide as captured by TEM.

Graphene oxide was reduced to form RGO employing hydrazine hydrate, and RGO was dispersed in water with ammonium hydroxide at a pH around 10 following a published procedure.[19] A mixture containing 5.0 mL of 0.125 wt % graphene oxide, 4.8 mL of double distilled water, 200 μL of hydrazine hydrate (50 wt %), and 35 μL of NH_4OH (28 wt %) was stirred for 5 min and heated at 95 °C for 1 h. The suspension containing RGO was subsequently dialyzed against distilled water to remove hydrazine and NH_4OH. RGO had a sheet height of 1.73 nm, which was determined by section analysis and confirmed that between three and five layers of RGO were present (Supporting Information, Figure S4c). The FT-IR spectrum for RGO (Supporting Information, Figure S6a) depicted a reduction in the O−H stretch around 3400 cm^{-1}, and carbonyl groups appeared around 1700 cm^{-1}. Figure 4a and Supporting Information, Figure S1c,d depicted the TEM micrograph of RGO, and the UV−vis spectrum of RGO displayed a shoulder around 327 nm (Supporting Information, Figure S6b).

Incubation with HRP and H_2O_2. Three vials were prepared by adding 2.0 mL of the 0.125 wt% graphene oxide dispersed in double distilled water. Lyophilized HRP type VI was solubilized in 1× phosphate buffered saline (PBS) (11.9 mM phosphates, 137 mM NaCl, and 2.7 mM KCl) at 0.390 mg mL^{-1} and added to two of the vials containing graphene oxide at a volume of 4.0 mL. This created two vials with a total volume of 6.0 mL (active and control I, $-H_2O_2$) and one with a total volume of 2.0 mL (control II, −HRP). Next, 3.5 mL, 4.0 mL, and 7.5 mL of 1 × PBS were added to active, control I, and control II, respectively, for a total volume of 9.5 mL, 10.0 and 9.5 mL. All vials were then sealed with a septum and wrapped with parafilm to create an airtight seal. The identical procedure was followed to prepare three vials for RGO. An additional control III vial (−graphene oxide) was created by adding 4.0 mL of HRP and 5.5 mL of 1 × PBS. A sample of 0.5 mL of 800 μM H_2O_2 was added by needle through the septum to the active, control II, and control III vials; this started the oxidation reaction. Daily additions of 4 μL of 0.1 M H_2O_2 were added to the active, control II, and control III vials; this was continued on a daily basis for 20 days.

Preparation of Holey Reduced Graphene Oxide (hRGO). A sample of holey graphene oxide subjected to 8 days of oxidation was reduced to form hRGO employing hydrazine hydrate in an aqueous suspension containing ammonium hydroxide at a pH around 10 following a published procedure (Supporting Information, Figure S1g).[19] A mixture containing 5.0 mL of 0.125 wt % holey graphene oxide, 4.8 mL of double distilled water, 200 μL of hydrazine hydrate (50 wt %), and 35 μL of NH_4OH (28 wt %) was stirred for 5 min and heated at 95 °C for 1 h. The suspension containing hRGO was subsequently dialyzed against distilled water with 0.5% NH_4OH to remove hydrazine. The FT-IR spectrum for hRGO (Supporting Information, Figure S6a) depicted a reduction in the O−H stretch around 3400 cm^{-1}, and carbonyl groups appeared around 1700 cm^{-1}. Moreover, the UV−vis spectrum demonstrated a well-defined peak around 327 nm (Supporting Information, Figure S6b).

Raman Spectroscopy. Samples were prepared by drop-casting approximately 20 μL of graphene oxide or RGO at days 0, 4, or 20 on a quartz microscope slide and drying. All spectra were collected on a Renishaw *inVia* Raman microscope using an excitation wavelength of 633 nm. Samples were scanned from 1000 to 3000 cm^{-1} to visualize the D and G bands. Spectra were collected with a 15 s exposure time and averaged across 5 scans per location; a total of 10 locations were selected per sample.

Transmission Electron Microscopy. Samples in PBS suspension were first centrifuged at 3400 rpm for 30 min and decanted of supernatant in order to effectively remove salt contributions from the buffer. The sample was resuspended into approximately 1 mL of double distilled H_2O by sonication for 1 min. One drop of the suspended sample was placed on a lacey carbon grid (Pacific-Grid Tech) and allowed to dry in ambient conditions for 2 h prior to TEM imaging (FEI Morgagni, 80 keV).

Atomic Force Microscopy (AFM). A Multimode scanning probe microscope (Veeco) was utilized in tapping mode for height, phase, and sectional analysis. Sample preparation was performed on freshly cleaved mica that was treated with approximately 20 μL of 0.1% (w/w) poly-L-lysine (aq) through spin-coating at 1400 rpm Approximately 10 μL of sample (aq) was spin-coated at 1400 rpm and allowed to dry in ambient for

45 min prior to imaging. Using a "supersharp" Si probe (tip radius < 5 nm, AppNano), tapping mode was performed at a drive frequency of 182.316 Hz, an amplitude set point of 0.2465 V, and a drive amplitude of 216 mV. Images were initially scanned in a 13.1 μm area prior to magnification of relevant areas. Postimaging processing included section analysis for quantifying cross-sectional heights of samples.

Polyacrylamide Gel Electrophoresis (PAGE). Four samples were analyzed using gel electrophoresis, which included a control for horseradish peroxidase (HRP, 1.1 mg) (around 44 kDa) without hydrogen peroxide (H_2O_2), HRP (1.1 mg) incubated for 3 h in the presence of H_2O_2 (final concentration of 40 μM H_2O_2 added every 1 h), and HRP (1.1 mg each) incubated with graphene oxide or reduced graphene oxide (RGO) for 3 h in the presence of H_2O_2 (final concentration of 40 μM H_2O_2 added every 1 h). Samples were separated by sodium dodecyl sulfate (SDS) PAGE in Tris-glycine buffer. The running gel contained 10% acrylamide, 0.375 mM tris-HCl buffer (pH 8.8), 0.1% SDS; the stacking gel contained 4% acrylamide, 0.125 mM tris-HCl buffer (pH 6.8), 0.1% SDS. Gels were polymerized by the addition of 0.1% ammonium persulfate and 0.1% TEMED. Running buffer included 250 mM tris, 250 mM glycine, 0.1% SDS. Samples were diluted in the loading buffer containing 0.125 mM tris-HCl (pH 6.8) and 1% SDS and boiled for 5 min. Electrophoresis was run at a constant voltage of 130 V. Gels were stained by a SilverSNAP kit according to the manufacturer's manual.

Enzymatic Kinetic Studies. Amplex Red was employed to measure the concentration of the substrate, H_2O_2, as a function of time for a constant concentration of HRP (0.390 mg mL^{-1}) incubated with graphene oxide (graphene oxide-active). At time t = 0, 4 μL of 0.1 M H_2O_2 was added to the sample for a final concentration of 40 μM. At 5 min time intervals (for 1 h), a 249 μL aliquot of sample and 1 μL of 10 mM Amplex Red was gently mixed, and the UV−vis spectrum of the sample was taken with 1 × PBS utilized as the background. Figure 5d contained the resulting concentration *vs* time plots for graphene oxide-active; the data was fitted with an exponential decay plot.

Gas Chromatography−Mass Spectrometry (GC−MS). Approximately 2 μL of sample headspace (total headspace volume: 5 mL) was injected into a Shimadzu QP5050A GC−MS unit equipped with an XTI-F capillary column by sampling through the septum of one of the five vials (graphene oxide-active, graphene oxide-control I, graphene oxide-control II, graphene oxide-control III, and RGO-active) on day 0 and day 10 of the oxidation study. A basic temperature program was performed, starting at 100 °C held for 1 min, followed by temperature ramping at a rate of 10 °C min^{-1} until a maximum temperature of 325 °C was achieved and held for an additional 10 min.

Fabrication and Measurement of Solution- and Back-Gated RGO and hRGO Field-Effect Transistors. Field-effect transistors (FETs) were fabricated using a standard photolithography process on Si/SiO_2 (oxide thickness = 200 nm). The Ti/Au metal contacts (Ti/Au = 30/100 nm) were deposited by electron beam evaporation. Individual graphene flakes were dielectrophretically deposited onto interdigitated electrodes at a frequency of 300 kHz and an ac field of 1.6 MV m^{-1},[52] and devices were annealed in vacuum at 180 °C for 2 h. The Si chips with graphene flakes were wire-bonded and packaged in a 40-pin ceramic dual-inline package. For backgate measurements, the Si substrate served as gate electrode. The electrical performance of the device was measured using two source measuring units (Keithley 2400). The gate potential was swept from −85 V to +85 V with a constant source drain voltage (V_{ds}) of 50 mV or from −20 V to +20 V with a constant source drain voltage (V_{ds}) of 10 mV.

For solution-gated measurements, a liquid gate potential was applied to Ag/AgCl (3 M NaCl) reference electrode. Epoxy resin was used to prevent direct contact between metal electrode and electrolyte, leaving active graphene area exposed to electrolyte solution. A small polymer chamber was placed on the chip and sealed with epoxy to hold a small volume (a few milliliters) of the electrolyte. Solution gate measurements were performed in 10 mM KCl/10 mM PBS (pH = 7), and the gate voltage was swept from −0.75 V to +0.75 V with the V_{ds} kept constant at 10 mV.

Molecular Modeling. HRP was docked to different chemical structures of RGO and graphene oxide. 3D structures of RGO and graphene oxide sheets with dimensions of 3 nm were generated using SketchEl molecular editing tool provided by the VegaZZ software package.[53] Where indicated, edges of RGO were modified to contain both carboxyl and carbonyl groups. In the case of graphene oxide, the basal plane always contained epoxide and hydroxyl groups, and the edges had a combination of carbonyl, carboxyl, lactol, and phenolic groups in accordance with previous work.[54,55] Using AutoDock Vina software,[56] docking of HRP's X-ray crystal structure (PDB ID: 1H5A, chain A) to both RGO and graphene oxide sheets was performed as described previously.[24] A grid box with dimensions of 120 Å in the *x*, *y*, and *z* directions was used with the center of the box placed at the center of the protein molecule. The resulting nine graphene ligand bound poses were further analyzed to find the most preferred binding pose in each case. The preferred binding pose was defined as the pose that has the minimum energy with the maximum number of poses clustered in that site.

Acknowledgment. This work was supported by NIEHS R01ES019304, NIOSH 0H008282, and the 7th Framework Program of the European Commission (EC-FP7-NANOMMUNE-214281). GPK acknowledges an EPA STAR Graduate Fellowship FP-91713801. This research was supported in part by Computational Resources on PittGrid (www.pittgrid.pitt.edu).

Supporting Information Available: Supplemental TEM micrographs for the graphene oxide and RGO experiments (Figure S1); Amplex Red assay for days 1 and 20 of RGO oxidation (Figure S2); electron paramagnetic resonance (EPR) spectroscopy data (Figure S3); AFM images with section analysis of graphene oxide, HRP, and RGO (Figure S4); details of the predicted interaction sites for RGO, graphene oxide, and holey graphene oxide on HRP (Table S1); backgate FET data for hRGO and RGO (Figure S5); and FT-IR and UV−vis spectra of hRGO, RGO, and graphene oxide (Figure S6). This material is available free of charge *via* the Internet at http://pubs.acs.org.

REFERENCES AND NOTES

1. Geim, A. K.; Novoselov, K. S. The Rise of Graphene. *Nat. Mater.* **2007,** *6*, 183–91.
2. Zhu, Y.; Murali, S.; Cai, W.; Li, X.; Suk, J. W.; Potts, J. R.; Ruoff, R. S. Graphene and Graphene Oxide: Synthesis, Properties, and Applications. *Adv. Mater.* **2010,** *22*, 3906–3924.
3. Lee, C.; Wei, X.; Kysar, J. W.; Hone, J. Measurement of the Elastic Properties and Intrinsic Strength of Monolayer Graphene. *Science* **2008,** *321*, 385–388.
4. Geim, A. K. Graphene: Status and Prospects. *Science* **2009,** *324*, 1530–1534.
5. Allen, M. J.; Tung, V. C.; Kaner, R. B. Honeycomb Carbon: A Review of Graphene. *Chem. Rev.* **2010,** *110*, 132–145.
6. Kauffman, D. R.; Star, A. Graphene *versus* Carbon Nanotubes for Chemical Sensor and Fuel Cell Applications. *Analyst* **2010,** *135*, 2790–2797.
7. Dreyer, D. R.; Park, S.; Bielawski, C. W.; Ruoff, R. S. The Chemistry of Graphene Oxide. *Chem. Soc. Rev.* **2010,** *39*, 228–240.
8. Park, S.; Ruoff, R. S. Chemical Methods for the Production of Graphenes. *Nat. Nanotechnol.* **2009,** *4*, 217–224.
9. Stankovich, S.; Dikin, D. A.; Dommett, G. H. B.; Kohlhaas, K. M.; Zimney, E. J.; Stach, E. A.; Piner, R. D.; Nguyen, S. T.; Ruoff, R. S. Graphene-Based Composite Materials. *Nature* **2006,** *442*, 282–286.
10. Tung, V. C.; Allen, M. J.; Yang, Y.; Kaner, R. B. High-Throughput Solution Processing of Large-Scale Graphene. *Nat. Nanotechnol.* **2009,** *4*, 25–29.
11. Schniepp, H. C.; Li, J.-L.; McAllister, M. J.; Sai, H.; Herrera-Alonso, M.; Adamson, D. H.; Prud'homme, R. K.; Car, R.; Saville, D. A.; Aksay, I. A. Functionalized Single Graphene Sheets Derived from Splitting Graphite Oxide. *J. Phys. Chem. B* **2006,** *110*, 8535–8539.
12. McAllister, M. J.; Li, J.-L.; Adamson, D. H.; Schniepp, H. C.; Abdala, A. A.; Liu, J.; Herrera-Alonso, M.; Milius, D. L.; Car, R.; Prud'homme, R. K.; *et al.* Single Sheet Functionalized Graphene by Oxidation and Thermal Expansion of Graphite. *Chem. Mater.* **2007,** *19*, 4396–4404.

13. Dreyer, D. R.; Ruoff, R. S.; Bielawski, C. W. From Conception to Realization: An Historial Account of Graphene and Some Perspectives for Its Future. *Angew. Chem., Int. Ed.* **2010,** *49*, 9336–9344.
14. Sun, X.; Liu, Z.; Welsher, K.; Robinson, J.; Goodwin, A.; Zaric, S.; Dai, H. Nanographene Oxide for Cellular Imaging and Drug Delivery. *Nano Res.* **2008,** *1*, 203–212.
15. Dikin, D. A.; Stankovich, S.; Zimney, E. J.; Piner, R. D.; Dommett, G. H. B.; Evmenenko, G.; Nguyen, S. T.; Ruoff, R. S. Preparation and Characterization of Graphene Oxide Paper. *Nature* **2007,** *448*, 457–460.
16. Li, S.-S.; Tu, K.-H.; Lin, C.-C.; Chen, C.-W.; Chhowalla, M. Solution-Processable Graphene Oxide as an Efficient Hole Transport Layer in Polymer Solar Cells. *ACS Nano* **2010,** *4*, 3169–3174.
17. Robinson, J. T.; Perkins, F. K.; Snow, E. S.; Wei, Z.; Sheehan, P. E. Reduced Graphene Oxide Molecular Sensors. *Nano Lett.* **2008,** *8*, 3137–3140.
18. Zhou, M.; Zhai, Y. M.; Dong, S. J. Electrochemical Sensing and Biosensing Platform Based on Chemically Reduced Graphene Oxide. *Anal. Chem.* **2009,** *81*, 5603–5613.
19. Li, D.; Mueller, M. B.; Gilje, S.; Kaner, R. B.; Wallace, G. G. Processable Aqueous Dispersions of Graphene Nanosheets. *Nat. Nanotechnol.* **2008,** *3*, 101–105.
20. Liu, L.; Ryu, S.; Tomasik, M. R.; Stolyarova, E.; Jung, N.; Hybertsen, M. S.; Steigerwald, M. L.; Brus, L. E.; Flynn, G. W. Graphene Oxidation: Thickness-Dependent Etching and Strong Chemical Doping. *Nano Lett.* **2008,** *8*, 1965–1970.
21. Tapaszto, L.; Dobrik, G.; Lambin, P.; Biro, L. P. Tailoring the Atomic Structure of Graphene Nanoribbons by Scanning Tunnelling Microscope Lithography. *Nat. Nanotechnol.* **2008,** *3*, 397–401.
22. Li, X.; Wang, X.; Zhang, L.; Lee, S.; Dai, H. Chemically Derived, Ultrasmooth Graphene Nanoribbon Semiconductors. *Science* **2008,** *319*, 1229–1232.
23. Allen, B. L.; Kichambare, P. D.; Gou, P.; Vlasova, I. I.; Kapralov, A. A.; Konduru, N.; Kagan, V. E.; Star, A. Biodegradation of Single-Walled Carbon Nanotubes through Enzymatic Catalysis. *Nano Lett.* **2008,** *8*, 3899–3903.
24. Allen, B. L.; Kotchey, G. P.; Chen, Y.; Yanamala, N. V. K.; Klein-Seetharaman, J.; Kagan, V. E.; Star, A. Mechanistic Investigations of Horseradish Peroxidase-Catalyzed Degradation of Single-Walled Carbon Nanotubes. *J. Am. Chem. Soc.* **2009,** *131*, 17194–17205.
25. Kagan, V. E.; Konduru, N. V.; Feng, W.; Allen, B. L.; Conroy, J.; Volkov, Y.; Vlasova, I. I.; Belikova, N. A.; Yanamala, N.; Kapralov, A.; *et al*. Carbon Nanotubes Degraded by Neutrophil Myeloperoxidase Induce Less Pulmonary Inflammation. *Nat. Nanotechnol.* **2010,** *5*, 354–359.
26. Dresselhaus, M. S.; Jorio, A.; Hofmann, M.; Dresselhaus, G.; Saito, R. Perspectives on Carbon Nanotubes and Graphene Raman Spectroscopy. *Nano Lett.* **2010,** *10*, 751–758.
27. Gorris, H. H.; Walt, D. R. Mechanistic Aspects of Horseradish Peroxidase Elucidated through Single-Molecule Studies. *J. Am. Chem. Soc.* **2009,** *131*, 6277–6282.
28. Welinder, K. G. Amino Acid Sequence Studies of Horseradish Peroxidase. *Eur. J. Biochem.* **1979,** *96*, 483–502.
29. Qian, S. Y.; Chen, Y. R.; Deterding, L. J.; Fann, Y. C.; Chignell, C. F.; Tomer, K. B.; Mason, R. P. Identification of Protein-Derived Tyrosyl Radical in the Reaction of Cytochrome C and Hydrogen Peroxide: Characterization by ESR Spin-Trapping, HPLC and MS. *Biochem. J.* **2002,** *363*, 281–288.
30. Detweiler, C. D.; Lardinois, O. M.; Deterding, L. J.; de Montellano, P. R. O.; Tomer, K. B.; Mason, R. P. Identification of the Myoglobin Tyrosyl Radical by Immunospin Trapping and Its Dimerization. *Free Radical Biol. Med.* **2005,** *38*, 969–976.
31. Ehrenshaft, M.; Mason, R. P. Protein Radical Formation on Thyroid Peroxidase During Turnover as Detected by Immunospin Trapping. *Free Radical Biol. Med.* **2006,** *41*, 422–430.
32. Trott, O.; Olson, A. J. Autodock Vina: Improving the Speed and Accuracy of Docking with a New Scoring Function, Efficient Optimization and Multithreading. *J. Comput. Chem.* **2010,** *31*, 455–461.
33. Filizola, M.; Loew, G. H. Role of Protein Environment in Horseradish Peroxidase Compound I Formation: Molecular Dynamics Simulations of Horseradish Peroxidase—HOOH Complex. *J. Am. Chem. Soc.* **2000,** *122*, 18–25.
34. Tuynman, A.; Spelberg, J. L.; Kooter, I. M.; Schoemaker, H. E.; Wever, R. Enantioselective Epoxidation and Carbon—Carbon Bond Cleavage Catalyzed by Coprinus Cinereus Peroxidase and Myeloperoxidase. *J. Biol. Chem.* **2000,** *275*, 3025–3030.
35. Ortiz de Montellano, P. R.; Grab, L. A. Cooxidation of Styrene by Horseradish Peroxidase and Phenols: A Biochemical Model for Protein-Mediated Cooxidation. *Biochemistry* **1987,** *26*, 5310–5314.
36. Novoselov, K. S.; Geim, A. K.; Morozov, S. V.; Jiang, D.; Katsnelson, M. I.; Grigorieva, I. V.; Dubonos, S. V.; Firsov, A. A. Two-Dimensional Gas of Massless Dirac Fermions in Graphene. *Nature* **2005,** *438*, 197–200.
37. Meric, I.; Han, M. Y.; Young, A. F.; Ozyilmaz, B.; Kim, P.; Shepard, K. L. Current Saturation in Zero-Bandgap, Top-Gated Graphene Field-Effect Transistors. *Nat. Nanotechnol.* **2008,** *3*, 654–659.
38. Nakada, K.; Fujita, M.; Dresselhaus, G.; Dresselhaus, M. S. Edge State in Graphene Ribbons: Nanometer Size Effect and Edge Shape Dependence. *Phys. Rev. B: Condens. Matter Mater. Phys.* **1996,** *54*, 17954.
39. Son, Y.-W.; Cohen, M. L.; Louie, S. G. Energy Gaps in Graphene Nanoribbons. *Phys. Rev. Lett.* **2006,** *97*, 216803.
40. Barone, V.; Hod, O.; Scuseria, G. E. Electronic Structure and Stability of Semiconducting Graphene Nanoribbons. *Nano Lett.* **2006,** *6*, 2748–2754.
41. Bai, J.; Zhong, X.; Jiang, S.; Huang, Y.; Duan, X. Graphene Nanomesh. *Nat. Nanotechnol.* **2010,** *5*, 190–194.
42. Kim, M.; Safron, N. S.; Han, E.; Arnold, M. S.; Gopalan, P. Fabrication and Characterization of Large-Area, Semiconducting Nanoperforated Graphene Materials. *Nano Lett.* **2010,** *10*, 1125–1131.
43. Liu, H.; Ryu, S.; Chen, Z.; Steigerwald, M. L.; Nuckolls, C.; Brus, L. E. Photochemical Reactivity of Graphene. *J. Am. Chem. Soc.* **2009,** *131*, 17099–17101.
44. Huang, J. Y.; Qi, L.; Li, J. *In Situ* Imaging of Layer-by-Layer Sublimation of Suspended Graphene. *Nano Res.* **2010,** *3*, 43–50.
45. Bieri, M.; Treier, M.; Cai, J.; Ait-Mansour, K.; Ruffieux, P.; Groning, O.; Groning, P.; Kastler, M.; Rieger, R.; Feng, X.; *et al*. Porous Graphenes: Two-Dimensional Polymer Synthesis with Atomic Precision. *Chem. Commun.* **2009,** 6919–6921.
46. Chen, F.; Qing, Q.; Xia, J.; Li, J.; Tao, N. Electrochemical Gate-Controlled Charge Transport in Graphene in Ionic Liquid and Aqueous Solution. *J. Am. Chem. Soc.* **2009,** *131*, 9908–9909.
47. Eda, G.; Fanchini, G.; Chhowalla, M. Large-Area Ultrathin Films of Reduced Graphene Oxide as a Transparent and Flexible Electronic Material. *Nat. Nanotechnol.* **2008,** *3*, 270–274.
48. Jung, I.; Dikin, D. A.; Piner, R. D.; Ruoff, R. S. Tunable Electrical Conductivity of Individual Graphene Oxide Sheets Reduced at "Low" Temperatures. *Nano Lett.* **2008,** *8*, 4283–4287.
49. Joung, D.; Chunder, A.; Zhai, L.; Khondaker, S. I., High Yield Fabrication of Chemically Reduced Graphene Oxide Field Effect Transistors by Dielectrophoresis. *Nanotechnology* 2010, *21*.
50. Salas, E. C.; Sun, Z.; Lüttge, A.; Tour, J. M. Reduction of Graphene Oxide *via* Bacterial Respiration. *ACS Nano* **2010,** *4*, 4852–4856.
51. Kovtyukhova, N. I.; Ollivier, P. J.; Martin, B. R.; Mallouk, T. E.; Chizhik, S. A.; Buzaneva, E. V.; Gorchinskiy, A. D. Layer-by-Layer Assembly of Ultrathin Composite Films from Micron-Sized Graphite Oxide Sheets and Polycations. *Chem. Mater.* **1999,** *11*, 771–778.
52. Vijayaraghavan, A.; Sciascia, C.; Dehm, S.; Lombardo, A.; Bonetti, A.; Ferrari, A. C.; Krupke, R. Dielectrophoretic Assembly of High-Density Arrays of Individual Graphene Devices for Rapid Screening. *ACS Nano* **2009,** *3*, 1729–1734.

53. Pedretti, A.; Villa, L.; Vistoli, G. Vega—An Open Platform to Develop Chemo-bio-informatics Applications, Using Plug-in Architecture and Script Programming. *J. Comput.-Aided Mol. Des.* **2004,** *18*, 167–73.
54. Lerf, A.; He, H.; Forster, M.; Klinowski, J. Structure of Graphite Oxide Revisited. *J. Phys. Chem. B* **1998,** *102*, 4477–4482.
55. Casabianca, L. B.; Shaibat, M. A.; Cai, W. W.; Park, S.; Piner, R.; Ruoff, R. S.; Ishii, Y. NMR-Based Structural Modeling of Graphite Oxide Using Multidimensional ^{13}C Solid-State NMR and *ab Initio* Chemical Shift Calculations. *J. Am. Chem. Soc.* **2010,** *132*, 5672–5676.
56. Trott, O.; Olson, A. J. Software News and Update Autodock Vina: Improving the Speed and Accuracy of Docking with a New Scoring Function, Efficient Optimization, and Multithreading. *J. Comput. Chem.* **2010,** *31*, 455–461.